Graphene surface plasmon polaritons transport on curved substrates

Ting-Hui Xiao, Lin Gan, and Zhi-Yuan Li*

Laboratory of Optical Physics, Institute of Physics, Chinese Academy of Sciences, P.O. Box 603, Beijing 100190, China
**Corresponding author: lizy@aphy.iphy.ac.cn*

Received June 17, 2015; revised August 27, 2015; accepted August 27, 2015;
posted August 27, 2015 (Doc. ID 243216); published October 1, 2015

We theoretically investigate the transport property of graphene surface plasmon polaritons (GSPPs) on curved graphene substrates. The dispersion relationship, propagation length, and field confinement are calculated by an analytical method and compared with those on planar substrates. Based on our theory, the bend of graphene nearly does not affect the property of GSPPs except for an extremely small shift to the lower frequency for the same effective mode index. The field distributions and the eigenfrequencies of GSPPs on planar and cylindrical substrates are calculated by the finite element method, which validates our theoretical analysis. Moreover, three types of graphene-guided optical interconnections of GSPPs, namely, planar to curved graphene film, curved to planar graphene film, and curved to curved graphene film, are proposed and examined in detail. The theoretical results show that the GSPPs propagation on curved graphene substrates and interconnections will not induce any additional losses if the phase-matching condition is satisfied. Additionally, the extreme tiny size of curved graphene for interconnection at a certain spectra range is predicted by our theory and validated by the simulation of 90° turning of GSPPs. The bending effect on the property of GSPPs is systematically analyzed and identified. Our studies would be helpful to instruct design of plasmonic devices involving curved GSPPs, such as nanophotonic circuits, flexible plasmonic, and biocompatible devices.

OCIS codes: (240.6680) Surface plasmons; (160.4670) Optical materials; (200.4650) Optical interconnects.
http://dx.doi.org/10.1364/PRJ.3.000300

1. INTRODUCTION

Surface plasmon polaritons (SPPs), the electromagnetic excitations propagating at the interface between a metal and a dielectric medium, have attracted considerable attention in a wide range of fields, owing to their extraordinary properties such as strong field confinement and enhancement [1]. A variety of novel and fascinating applications based on SPPs also have been demonstrated [2–6]. However, with further progress in theoretical and experimental research, the bottleneck of conventional SPPs on the surface of noble metals emerges. The high ohmic loss and weak tunability of noble metals limit their applicability and performance [7].

In recent years, graphene, an atomically thin carbon layer with superior electronic and optical properties [8], has become an available plasmonic material with high potential [9]. Compared with noble metals, graphene surface plasmon polaritons (GSPPs) display some superior characteristics such as ultracompact electromagnetic field confinement, low loss, and strong tunability. Therefore, a great number of applications harnessing GSPPs have been proposed. For example, a widely tunable far-infrared notch filter and terahertz linear polarizer using graphene/insulator stacks [10] have been experimentally realized. Terahertz metamaterial consisting of graphene micro-ribbon arrays [11] displays its tunability over a broad frequency range and prominent optical absorption at room temperature. Transformation optics using graphene [12,13] conveniently tailors electromagnetic fields into desired spatial patterns by varying the chemical potential of graphene. Additionally, graphene surface plasmon-based infrared modulator, highly sensitive biosensor, and electrically tunable antenna [14–16] also have been presented.

Graphene also possesses remarkable mechanical flexibility [17], which enables graphene to realize flexible plasmonic devices. In these years, wearable or biocompatible devices utilizing flexible materials have received intensive concern. Continued advances in this field have been designed to realize electronic or photonic components with excellent performance on flexible, nonplanar, or even biocompatible substrates [18]. Thus, graphene is undoubtedly a suitable potential alternative, especially taking its unique property of SPPs into consideration. Several optical applications utilizing the combination of flexibility and SPPs property of graphene have been proposed, such as a graphene nanoribbon splitter and waveguide [19], plasmonic switch, and frequency demultiplexer [20]. However, how the bend will affect the property of GSPPs when graphene is on flexible or nonplanar substrate is still unclear, which hinders further development of flexible plasmonic devices by using graphene. Thus, the problem deserves to be investigated in depth.

In this paper, the property of GSPPs on curved substrates is systematically investigated. GSPPs on a cylindrical substrate (curved substrate with a fixed radius) as a concise and universal model are studied by an analytical method, which we developed. The dispersion relationship and propagation length of our model system are calculated and compared with those on planar substrate. Moreover, the field distributions and the eigenfrequencies of GSPPs on planar and curved substrates are calculated by means of the finite element method (FEM). As an extension to our theory, the GSPPs properties

of planar and curved graphene are also compared. Additionally, several simple elements comprising graphene nanophotonic interconnections based on GSPPs are proposed and simulated by our theoretical and numerical tools. In particular, the extreme tiny size of curved graphene, which still allows for efficient interconnection of GSPPs at a certain spectra range, is predicted by our theory and verified by our simulation. Generally, how the bend will affect the property of GSPPs is systematically analyzed and identified.

This paper is arranged as follows. In Section 2, we present our theoretical model and analytical theory. In Section 3, transport properties of GSPPs on curved substrates—including the dispersion relationship, propagation length, field confinement, and modal field distributions—are calculated and compared with those on planar substrates based on our theory. In Section 4, various interconnections of GSPPs consisting of several simple elements are proposed and simulated by our theoretical and numerical tools. In Section 5, transport of GSPPs through a sharp bend is investigated. The extreme tiny size for efficient transport is predicted by our theory and validated by the simulation. Finally, in Section 6, we provide a summary and conclusion.

2. THEORETICAL MODEL AND FORMALISMS

Because a flexible and nonplanar surface can be decomposed into small curved surfaces with different curvature radii, the transport property of GSPPs on a curved surface with a certain curvature radius becomes a basic problem that can probe the transport property of GSPPs on an arbitrary curved surface. Therefore, we consider graphene deposited on a cylindrical substrate with radius a and refractive index m, as shown in Fig. 1. The cylindrical substrate is made of a homogeneous, isotropic, and nondispersive dielectric medium and placed in air. Graphene is treated as an infinitesimally thin layer characterized by a surface conductivity σ determined by Kubo formula [21]. The effective relaxation time of graphene is set as 0.1 ps, and the temperature is set as 300 K. The chemical potential of graphene is fixed to 0.8 eV. These parameters come from the experiment results [10,22]. According to the calculation of Kubo formula, the imaginary part of conductivity σ is positive at the wavelength ranging from 1.5 to 20 μm. Therefore, in this range, the planar graphene layer can only support TM surface plasmon modes. For this reason, we confine our investigation to the TM modes.

In the case of TM modes, there are only three field components H_z, E_r, and E_ϕ in the cylindrical polar coordinate system. The field components H_{cz}, E_{cr}, and $E_{c\phi}$ in the cylindrical substrate, namely, the interior space of the cylinder, can be expanded in the cylindrical coordinate system as

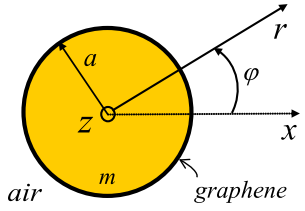

Fig. 1. Schematic of the theoretical model for GSPPs transporting on graphene deposited on a cylindrical substrate.

$$
\begin{aligned}
H_{cz} &= m\sum_{n=-\infty}^{\infty} G_n J_n(mk_0 r)\cdot e^{in\phi},\\
E_{cr} &= -\frac{1}{i\omega\varepsilon_m r}\frac{\partial H_{cz}}{\partial\phi} = -\frac{nm}{\omega\varepsilon_m r}\sum_{n=-\infty}^{\infty} G_n J_n(mk_0 r)\cdot e^{in\phi},\\
E_{c\phi} &= \frac{1}{i\omega\varepsilon_m}\frac{\partial H_{cz}}{\partial r} = \frac{k_0}{i\omega\varepsilon_0}\sum_{n=-\infty}^{\infty} G_n J_n'(mk_0 r)\cdot e^{in\phi},
\end{aligned}
\tag{1}
$$

where G_n is the expansion coefficient of internal field, J_n is the Bessel function of the first kind of integral order n, k_0 is the wave number in air, ω is the angular frequency, ε_0 is the vacuum permittivity, and ε_m is the permittivity of the cylindrical substrate. Meanwhile, the field components H_{sz}, E_{sr}, and $E_{s\phi}$ in the space outside the cylindrical substrate also can be expanded in the cylindrical coordinate system as

$$
\begin{aligned}
H_{sz} &= \sum_{n=-\infty}^{\infty} F_n H_n(k_0 r)\cdot e^{in\phi},\\
E_{sr} &= -\frac{1}{i\omega\varepsilon_0 r}\frac{\partial H_{sz}}{\partial\phi} = -\frac{n}{\omega\varepsilon_0 r}\sum_{n=-\infty}^{\infty} F_n H_n(k_0 r)\cdot e^{in\phi},\\
E_{s\phi} &= \frac{1}{i\omega\varepsilon_0}\frac{\partial H_{sz}}{\partial r} = \frac{k_0}{i\omega\varepsilon_0}\sum_{n=-\infty}^{\infty} F_n H_n'(k_0 r)\cdot e^{in\phi},
\end{aligned}
\tag{2}
$$

where F_n is the expansion coefficient of the external field and H_n is the Hankel function of integral order n. Applying the boundary condition at $r = a$, we obtain,

$$
\begin{aligned}
\hat{e}_r\times(\vec{E}_{s\phi}-\vec{E}_{c\phi}) &= 0,\\
\hat{e}_r\times(\hat{H}_{sz}-\hat{H}_{cz}) &= \sigma\vec{E}_{c\phi},
\end{aligned}
\tag{3}
$$

where a is the radius of cylindrical substrate; we also can obtain a matrix equation by substituting Eq. (1) and Eq. (2) into Eq. (3) as follows:

$$
\begin{pmatrix}
\frac{k_0}{i\omega\varepsilon_0}H_n'(k_0 r) & -\frac{k_0}{i\omega\varepsilon_0}J_n'(mk_0 r)\\
H_n(k_0 r) & -\frac{\sigma k_0}{i\omega\varepsilon_0}J_n'(mk_0 r)-mJ_n(mk_0 r)
\end{pmatrix}
\begin{pmatrix} F_n\\ G_n\end{pmatrix} = 0.
\tag{4}
$$

Then, the secular equation can be written as

$$
\begin{vmatrix}
\frac{k_0}{i\omega\varepsilon_0}H_n'(k_0 r) & -\frac{k_0}{i\omega\varepsilon_0}J_n'(mk_0 r)\\
H_n(k_0 r) & -\frac{\sigma k_0}{i\omega\varepsilon_0}J_n'(mk_0 r)-mJ_n(mk_0 r)
\end{vmatrix} = 0.
\tag{5}
$$

And the modal eigenequation can be acquired by simplifying Eq. (5) as follows:

$$
m\frac{J_n(mk_0 a)}{J_n'(mk_0 a)}-\frac{H_n(k_0 a)}{H_n'(k_0 a)}+\frac{i\sigma k_0}{\omega\varepsilon_0} = 0,
\tag{6}
$$

where the wavenumber k_0 is a complex number and equals to ω/c, and c is the velocity of light in vacuum. Thus, the GSPPs dispersion relationship and propagation length on cylindrical substrate can be calculated by solving the eigenequation. For the propagation of GSPPs on cylindrical substrate with a certain curvature radius a, the integer n determines the real part of the wavenumber of GSPPs in Eq. (6) due to the implicit continuous boundary condition that leads to the recirculating of GSPPs along the perimeter of cylindrical substrate. Thus, the wavenumbers of GSPPs and the dispersion relationship points corresponding to different eigenmodes and calculated by Eq. (6) should be discrete. The real part of the GSPPs wavenumber is $\mathrm{Re}(k_{\mathrm{GSPP}}) = n/a$. When parameters a and n

are determined, we can obtain the complex wavenumber k_0 by solving Eq. (6). The imaginary part of the GSPPs wavenumber can be calculated as $\mathrm{Im}(k_{\mathrm{GSPP}}) = \mathrm{Im}(k_0)\mathrm{Re}(k_{\mathrm{GSPP}})/\mathrm{Re}(k_0)$, and the frequency f equals to $\mathrm{Re}(k_0)c/2\pi$. Compared with the GSPPs on cylindrical substrate, the dispersion relationship of GSPPs on planar substrate can be calculated by the equation [23],

$$\frac{\varepsilon_0}{\sqrt{k_0^2 - k^2\varepsilon_0}} + \frac{\varepsilon_m}{\sqrt{k_0^2 - k^2\varepsilon_m}} + \frac{i\sigma}{\omega\varepsilon_0} = 0, \tag{7}$$

where $k = 2\pi f/c$ is the propagating wavenumber in air, and f is the frequency of the propagating wave.

3. TRANSPORT OF GSPPS ON CURVED SUBSTRATES

First, we can calculate the field distributions of GSPPs on cylindrical substrate by our above noted analytical method. As GSPPs in our model are TM waves, the magnetic field distribution can reflect the information of magnitude and phase. The distribution of the eigen-magnetic field H_z can be calculated by applying Eqs. (1) and (2). The relationship of the expansion coefficients of internal and external fields can be obtained by Eq. (4). Assuming the refractive index of the cylindrical substrate is 1.45 and the radius is 50 nm, the magnetic field distributions of the first six orders are depicted in Fig. 2. It clearly shows that the parameter n determines the wavenumbers along the perimeter of cylindrical substrate, which is consistent with our theoretical analysis above. The mode area decreases with the increase of n.

Because the field distributions of GSPPs on cylindrical substrate are calculated as previously noted, it then can be straightforward to find the dispersion relationship, propagation length, and field confinement of GSPPs on cylindrical substrates and make a comparison with those on planar substrates. By solving Eq. (6), we calculate the dispersion relationship of the first 20 order modes on cylindrical substrates whose refractive index is 1.45 and whose radius equals to 5, 50, and 500 nm, respectively. In comparison, the dispersion relationship of GSPPs on a planar substrate is also calculated by applying Eq. (7). The results are shown in Fig. 3. Figure 3(a) illustrates the relationship between the effective mode index and the frequency. As the real part of the GSPPs wavenumber is $\mathrm{Re}(k_{\mathrm{GSPP}}) = n/a$, the effective mode index can be expressed as $n_{\mathrm{eff}} = \mathrm{Re}(k_{\mathrm{GSPP}})/\mathrm{Re}(k_0)$, which equals to $n/[\mathrm{Re}(k_0)a]$. It can be seen from the figure that the discrete dispersion points, which correspond to the dispersion relationship for the different modes on cylindrical substrate, almost coincide with the black curve, which is the dispersion relationship on planar substrate. The dispersion points of GSPPs on curved substrate only have an extremely small shift to the lower frequency for the same effective mode index compared with those on planar substrate. This result suggests that the bend of graphene nearly does not affect the dispersion relationship of GSPPs, even if the radius of substrate decreases to the nanometer scale.

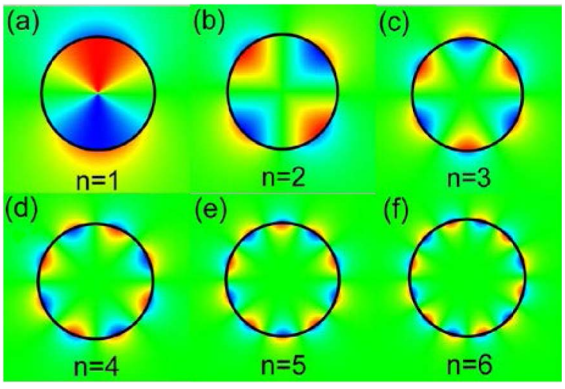

Fig. 2. GSPP magnetic field (H_z) distributions of first six order modes on cylindrical substrate. Radius of the cylindrical substrate is 50 nm.

Additionally, Fig. 3(b) demonstrates the relationship between relative propagation length and the frequency. The relative propagation length is defined as $L_{\mathrm{GSPP}}/\lambda_{\mathrm{GSPP}}$, where $L_{\mathrm{GSPP}} = 1/\mathrm{Im}(k_{\mathrm{GSPP}})$ and $\lambda_{\mathrm{GSPP}} = 2\pi/\mathrm{Re}(k_{\mathrm{GSPP}})$. Similar to Fig. 3(a), the discrete points representing the propagation length of GSPPs at a certain frequency on cylindrical substrate also almost coincide with the black curve representing the propagation length on planar substrate. The result suggests that the bend of graphene will not increase the propagation loss of GSPPs, and GSPPs on curved substrate can propagate as far as on planar substrate. The propagation length is dozens of λ_{GSPP} when the chemical potential of graphene is as high as 0.8 eV. In total, it indicates that GSPPs can nearly smoothly propagate on curved substrate as it does on planar substrate. Such a result can be attributed to the strong field confinement caused by graphene. Figures 3(c) and 3(d), respectively, demonstrate the GSPP decay lengths in air and the substrate whose refractive index is 1.45. The decay length, which reflects the degree of field confinement, is defined as $1/\mathrm{Re}(\sqrt{k_{\mathrm{GSPP}}^2 - \mathrm{Re}(k_0)^2})$. As the refractive index of the substrate is not significant and the field confinement is really strong, the curves of decay lengths in air and the substrate have little distinction. Moreover, Fig. 3 illustrates that the GSPPs mode points of the substrates with different radii coincide. For example, the second-order mode of the substrate with the radius of 5 nm coincides with the twentieth-order mode of the substrate with the radius of 50 nm. This also proves that the bend of graphene nearly does not affect the propagation of GSPPs.

In order to confirm our above conclusion, we calculate the field distributions of GSPPs on substrates with different radii by FEM. As is illustrated in Fig. 4, there are two cylindrical substrates with different radii but the same refractive index of 1.45. The radius of the larger cylindrical substrate is 50 nm, which is twice that of the smaller one. The eigenmodes of the GSPPs on these two cylindrical substrates are calculated at the same eigenfrequency. Figure 4(a) shows that the GSPPs on the smaller cylindrical substrate are at the second-order mode when the GSPPs on the larger cylindrical substrate are at the fourth-order mode. Figure 4(b) demonstrates the same relationship for the third- and sixth-order modes of graphene on these two substrates at a higher frequency. In other words, the perimeter of the larger substrate equals to four GSPPs wavelengths while the perimeter of the smaller one equals to two GSPPs wavelengths. As the perimeter of the larger cylindrical substrate is also twice that of the smaller one, it can be concluded that the GSPPs wavelengths for the substrates with different radii are the same. Therefore, the simulation results confirm that the bending degree of

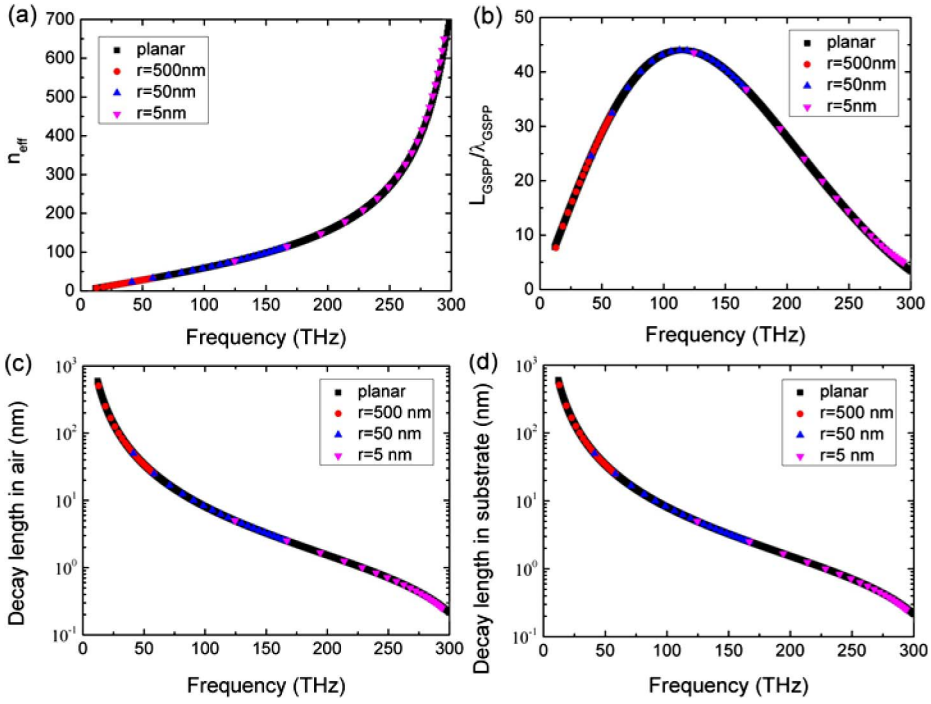

Fig. 3. (a) Dispersion relationship, (b) propagation length, and (c) decay lengths in air and (d) substrate of GSPP on planar substrate and on cylindrical substrates whose radii are 500, 50, and 5 nm, as illustrated. Discrete points of each color, which represent the correspondent values of GSPP on the cylindrical substrates with different radii, are the first 20 order modes.

graphene nearly does not affect the dispersion and propagation of GSPPs, especially when the difference of the bending degrees is not significant.

Factually, even though the bend of graphene nearly does not affect the dispersion and propagation of GSPPs, there still exists an extremely small variation. According to our above theory, the frequency of GSPPs for the same effective mode index on the curved substrate is a little lower than that on planar substrate. For further confirmation of our theory, we simulate the field distributions of GSPPs on planar substrate and on cylindrical substrate with the radius of 5 nm. The length of the plane substrate equals to the perimeter of cylindrical substrate. The refractive indices of the substrates are 1.45. We further calculate the eigenfrequencies of GSPPs on these two substrates based on our simulation. In Fig. 5, GSPPs can be excited on the cylindrical substrate but not on the planar substrate at 194.3 THz. On the contrary, for the same effective mode index, GSPPs can be excited on the planar substrate but not on the cylindrical substrate at 194.4 THz. This result illustrates that a small distinction of dispersion does exist between the GSPPs on planar and curved substrates. However, the difference of the frequencies is only 0.1 THz, even if the difference of the bending degrees is big. The simulation result that the frequency of GSPPs on curved substrate is a little lower than that on planar substrate for the same effective mode index is consistent with our analytical theory.

Additionally, we explore the GSPPs properties of curved and planar graphene in air. The length of the graphene is finite so that the edge effect is taken into consideration. As an extension of our theory, the substrate of this case can be considered as air. The lengths of the curved and planar graphene are equal. The radius of curvature of the curved graphene is

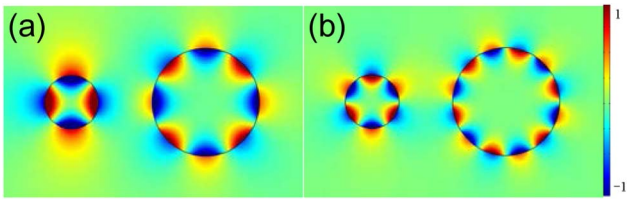

Fig. 4. GSPPs magnetic field (H_z) distributions at the same eigenfrequency on the cylindrical substrates with different radii. (a) and (b), respectively, correspond to 81.5 and 92.7 THz. Radius of the cylindrical substrate on the right is 50 nm, which is twice that of the left one in both (a) and (b).

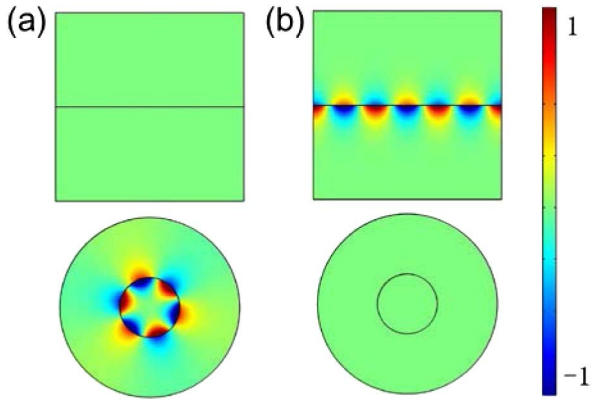

Fig. 5. Comparison of the GSPP magnetic field (H_z) distributions of the same GSPP wavelength (λ_{GSPP}) on the planar and cylindrical substrates. Lengths of graphene on the planar and cylindrical substrates are equal. Radius of the cylindrical substrate is 5 nm. Frequency is (a) 194.3 and (b) 194.4 THz.

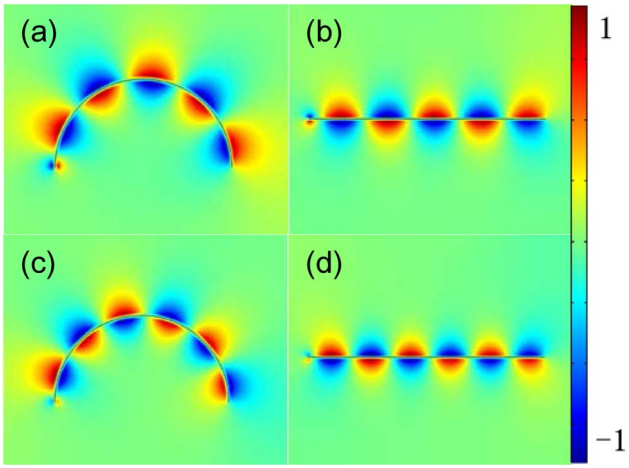

Fig. 6. GSPP magnetic field (H_z) distributions on planar and curved graphene films excited by the electric dipoles with different frequencies. (a) and (b) are excited at 110 THz, while (c) and (d) are excited at 120 THz. Lengths of planar and curved graphene films are equal. Curvature radius of the curved graphene film is 50 nm.

50 nm. We simulate the field distributions the curved and planar GSPPs excited by electric dipoles with different frequencies. Figures 6(a) and 6(b) are the field patterns excited by the electric dipoles with the frequency of 110 THz, while Figs. 6(c) and 6(d) correspond to 120 THz. All the electric dipoles are placed at the left edges of the graphene films. The results in Fig. 6 demonstrate that the GSPPs wavelengths of curved and planar graphene are equal at the same excited frequency, which once again indicates the dispersion is not affected by the bend of graphene. The simulation proves the reliability and usability of our theory in practice.

The result indicates that the wavenumbers of GSPPs on planar and curved graphene films, including real and imaginary parts, are consistent for a certain frequency. It is the basis for which the phase matching condition is achievable between the interconnections of decomposed curved surfaces with different curvature radii on flexible and nonplanar substrates. Therefore, if the flexible and nonplanar surfaces are continuously curved surfaces, which satisfy phase matching conditions everywhere on the graphene film, the properties of GSPPs on flexible and nonplanar substrates will be consistent with that on planar substrates. If the phase matching condition is not satisfied, it will induce reflection or interconnection loss for the propagation of GSPPs. This conclusion can be instructive for the application of GSPPs on flexible and nonplanar substrates.

4. INTERCONNECTION OF GSPPs ON CURVED SUBSTRATES

Because all the theoretical calculations and simulations above come to the conclusion that the bend of graphene does not affect the dispersion and propagation of GSPPs, the unique property of GSPPs can be exploited for many applications such as flexible plasmonic devices and nanophotonic circuits. In the following, we will show that graphene can realize excellent interconnections based on surface plasmons. First, a U-shaped curved graphene film and a planar graphene film that support the propagation of GSPPs are compared and demonstrated in Figs. 7(a) and 7(b). The GSPPs on the graphene films are excited by electric dipoles, which are, respectively, placed at the lower edge for the U shape and the left edge for the planar one. The lengths of the U shaped and planar graphene films are both equal to 357 nm. The curvature radius of the curved part in U shape is 50 nm. It can be observed that the fields are closely confined at the surface of graphene so that GSPPs easily adapt to the transition from curved to planar graphene or from planar to curved graphene. It seems from the field distributions that the bend of graphene and the interconnection between curved and planar films nearly do not affect the propagation of GSPPs.

The transmission spectra of these two shaped films are also calculated to verify what it seems like. In order to avoid the edge effect of the films but involve the influence of interconnection between curved and planar GSPPs films, we select two positions that are, respectively, at a distance of 50 nm away from the two edges of the graphene films and calculate the magnitudes of electric fields at these two positions. The transmission coefficient illustrated in Fig. 7(c) is defined as the ratio of electric field intensities of the two selected positions. The transmission spectra ranging from 190 to 200 THz are corresponding to telecommunication wavelengths. It can be observed from Fig. 7(c) that the transmission spectra of GSPPs on U-shaped and planar graphene films coincide well, which proves that the bend of graphene nearly does not affect the transport of GSPP. Moreover, the interconnection

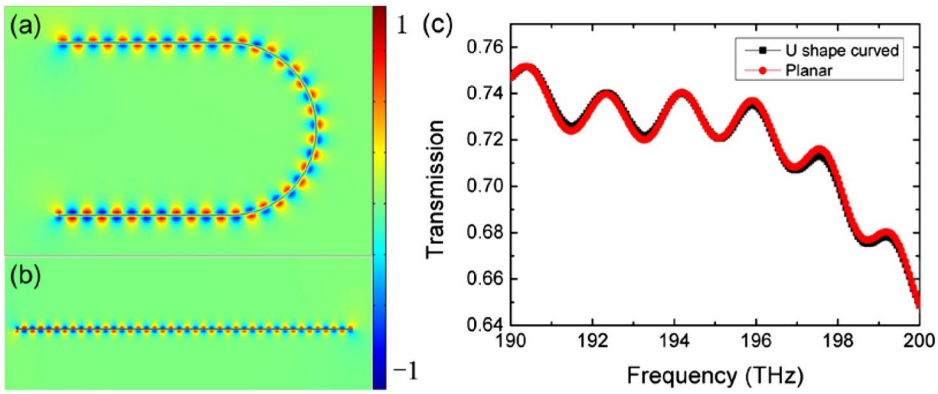

Fig. 7. Comparison of GSPP propagating on (a) U-shaped and (b) planar graphene films. GSPPs in (a) and (b) are excited by the electric dipoles with the frequency of 199 THz. Length of U-shaped graphene film is equal to that of the planar. Curvature radius of the curved part in a U-shaped film is 50 nm. (c) GSPP transmission spectra of these two shapes of graphene films.

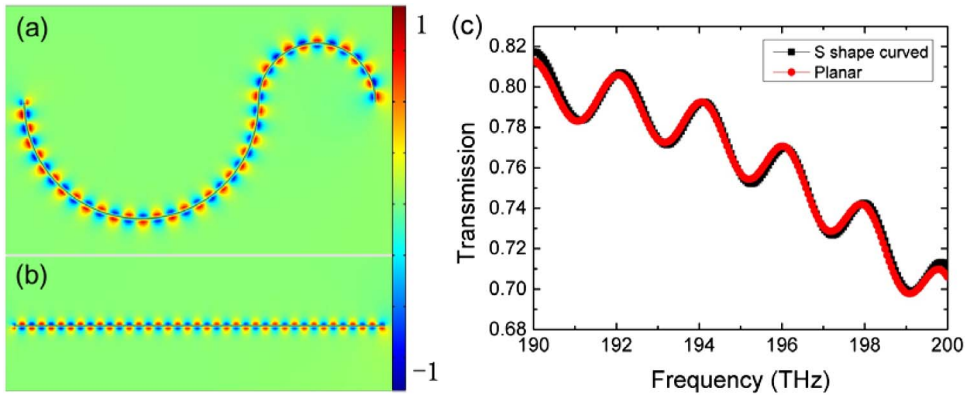

Fig. 8. Comparison of GSPP propagating on (a) S-shaped and (b) planar graphene films. GSPPs in (a) and (b) are excited by the electric dipoles with the frequency of 199 THz. Length of S-shaped graphene film is equal to that of the planar. The curvature radii of the two curved graphene films connected in an S shape are 35 and 70 nm. (c) GSPP transmission spectra of GSPPs on these two shapes of graphene films.

between the planar and curved graphene will not induce additional loss when the condition of phase matching at the interconnection position is satisfied. Thus, if the GSPPs interconnection is designed properly based on our theory, the transport of GSPPs to make a U-turn can be easily realized. Due to the low loss propagation of GSPPs and the weak reflection at the edge of the film, the graphene film also acts as a cavity along the propagation direction of GSPPs. Thus, the oscillation of transmission spectra in Fig. 7(c) is the result of the cavity modulation. The difference of frequencies between adjacent peaks equals to the longitudinal mode spacing of the cavity. Therefore, if the curved interconnection is poor, so that it induces strong reflection and interconnection loss, the longitudinal mode spacing and transmission value will alter by comparison with the planar case.

Moreover, S- and G-shaped curved GSPPs interconnections compared with the planar are studied and illustrated in Figs. 8 and 9, respectively. Similar to the study of the U shape, the GSPPs are excited at the edge of the graphene film by electric dipoles. The excited dipoles for S- and G-shaped interconnections are placed at the left edges. Two curved graphene films, whose curvature radii are 35 and 70 nm, are interconnected to form an S or G shape, as illustrated in Figs. 8(a) and 9(a), respectively. It can be seen from the field patterns that the propagation of GSPPs is nearly not affected by the variation of the bending degree. GSPPs can smoothly propagate along the graphene films. The transmission spectra of GSPPS on these two shaped films are also calculated. The positions used to calculate the magnitude of the electric field are selected at a distance of away from the two edges of the graphene films, where the curvature radius of the curved graphene are the selected positions are located. The field patterns for the reference planar graphene films with the equal lengths to that of the S and G shape are shown in Figs. 8(b) and 9(b), respectively. The distances of selected positions for the planar film are equal to that of the S and G shape. The transmission also is defined as the ratio of the electric field intensity at the selected positions. The transmission spectra in Figs. 8(c) and 9(c), respectively, reflect the comparison of the GSPPs transport on the S shape versus the planar and the G shape versus the planar. The coincidence of transmission curves once again proves that the bend of graphene nearly does not affect the propagation of GSPPs, and the interconnection of curved graphene with different radii and forms such as G and S shape will not add more loss as the phase matching condition is satisfied. It also can be seen that, as the lengths

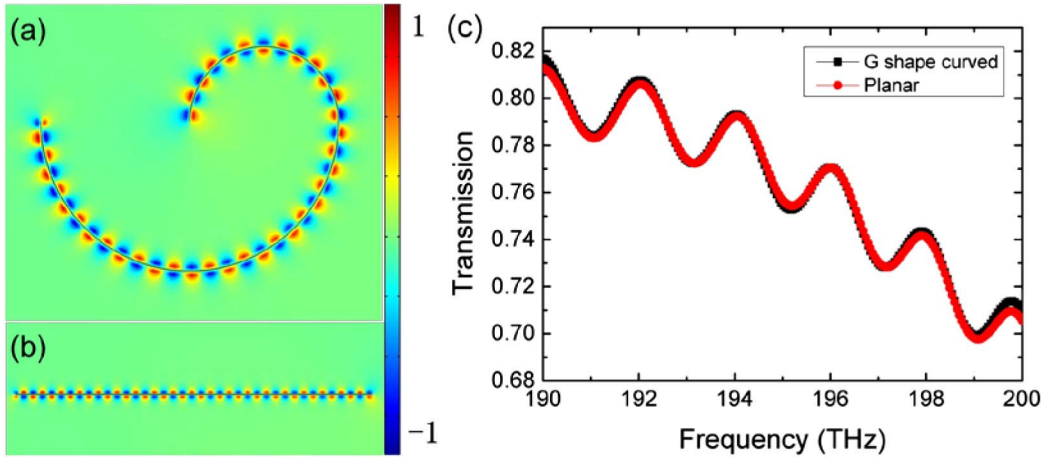

Fig. 9. Comparison of GSPP propagating on (a) G shape and (b) graphene films. GSPPs in (a) and (b) are excited by the electric dipoles with the frequency of 199 THz. Length of G-shaped graphene film is equal to that of the planar. The curvature radii of the two curved graphene films connected in the G shape are 35 and 70 nm. (c) GSPP transmission spectra of GSPPs on these two shapes of graphene films.

of S- and G-shaped films are equal, the transmission spectra ranging from 190 to 200 THz modulated by the formed cavity are equal. However, because the length of U-shaped graphene film is bigger than that of the S and G shape, the transmission spectra are different at the same frequency range.

Even though these interconnections are in different types, they all satisfy the phase matching condition, and the dispersion of GSPPs is nearly not affected by the bend. Therefore, they all do not induce additional reflection and interconnection loss. All the above simulations not only confirm our theory but also demonstrate the potential that highly doped graphene films can realize nanophotonic interconnections without inducing bending effect and interconnection loss.

5. TRANSPORT OF GSPPs THROUGH SHARP BENDS

We further investigate an interesting and important problem: What is the extreme size of curved graphene for interconnection at a certain spectra range? To answer this question, we consider transport of GSPPs through a series of 90° sharp bends, which are made from a quarter-circle-shaped curved graphene film with different curvature radius interconnecting two orthogonal planar graphene films. The spectral range for study of the 90° turning efficiency of GSPPs is still from 190 to 200 THz, which corresponds to telecommunication wavelengths.

Based on our above analytical theory, it can be seen from Fig. 3 that, when the radius is down to 5 nm, only the third-order mode for graphene on cylindrical substrate (circle shape) exists at the considered spectral range. Nevertheless, only if the length of curved graphene film is bigger than one wavelength of GSPPs, the modal profile of GSPPs is almost not distorted by the interconnection, and the phase matching condition can be satisfied. Thus, a quarter-circle-shaped graphene film with the curvature radius of 5 nm cannot efficiently realize interconnection at this spectral range. It can be inferred that the minimum radius should be about 7 nm, as the bending degree will not affect the dispersion and propagation of GSPPs. Additionally, because the refractive index of substrate used in Fig. 3 is 1.45, which is higher than that of air substrate, the minimum radius for the quarter-circle-shaped graphene film to excellently realize 90° turning of GSPPs in air is about 10 nm.

According to our above-noted theoretical analysis, we simulate the transport of GSPPs on two planar graphene films interconnected by the quarter-circle-shaped graphene (L shape). As comparisons, planar graphene films with equal lengths to those of the L shape are also simulated. Moreover, the transmission spectra of GSPPs on these two shaped graphene films are calculated and compared, which can better monitor the variation of propagation. The simulation results are illustrated in Fig. 10. The magnetic field (H_z) distributions in these figures are all excited by the dipoles with the frequency of 198 THz. In Fig. 10, the curvature radius of the quarter-circle-shaped graphene used to interconnect is 10 nm. The excitation dipoles for the L shape and planar graphene films are, respectively, placed at the upper edge and left edge of the films in the figures. Similar to the other shaped graphene film interconnections, we still select two positions, which are located, respectively, at a distance of 35 nm away from the two edges of the films along the propagation direction of GSPPs, to calculate the transmission spectra. The transmission is still defined as the ratio of intensities of electric fields at the selected positions. The length of each planar graphene film comprising the L shape is 157.5 nm. The comparison of field distributions in Figs. 10(a) and 10(b) and the coincidence of transmission spectra of these two shapes in Fig. 10(c) indicate that realization of 90° turning of GSPPs by utilizing a quarter-circle-shaped graphene film with curvature radius of 10 nm can be excellently achieved.

6. SUMMARY

In summary, we have theoretically investigated the property of GSPPs on curved substrate. GSPPs on the curved substrate with a constant radius (cylindrical substrate) as a concise and universal model are studied by an analytical method we have developed. The dispersion relationship, propagation length, and field confinement of the model are calculated and compared with those on planar substrates. According to our theoretical analysis, the bend of graphene nearly does not affect the property of GSPPs, including the dispersion relationship, propagation length, and field confinement. The dispersion curve of GSPPs on curved substrate only has an extremely

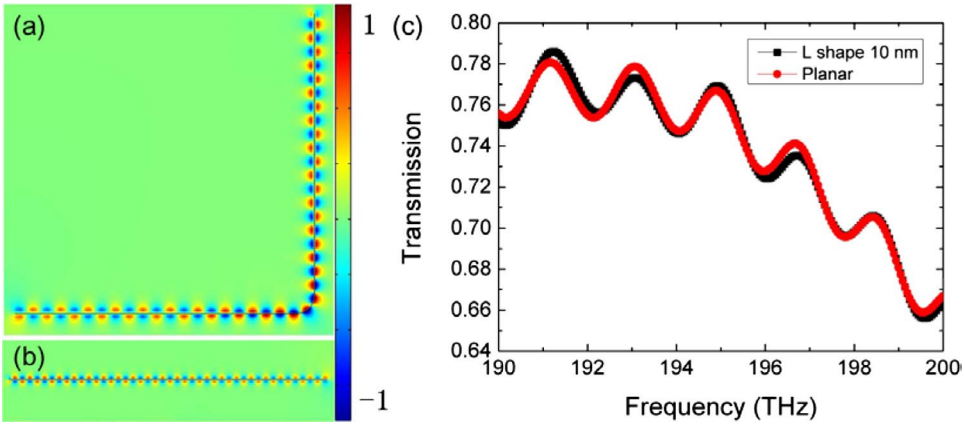

Fig. 10. Realization of 90° turning of GSPP by utilizing curved graphene. GSPPs in panels (a) and (b) are excited by the electric dipoles with the frequency of 198 THz. Curvature radius of the quarter-circle-shaped graphene film that is used to interconnect the two planar films is 10 nm in panel (a). As a comparison, the transport of GSPPS on a planar graphene film with the equal length to that of the L shape is illustrated in panel (b). (c) GSPP transmission spectra of these two shapes of graphene films.

small shift to the lower frequency for the same effective mode index compared with that on planar substrate. In order to validate our theory, we calculate the field distributions and the eigenfrequencies of GSPPs on planar and cylindrical substrates by means of FEM. The simulation results are consistent with our theoretical analysis.

In addition, different shapes of graphene film interconnections for realizing the transport of GSPPs are proposed and simulated. The simulation results demonstrate the great potential that highly doped graphene can realize nanophotonic interconnetions by making use of the property of curved GSPPs. Moreover, we predict the extreme tiny size of curved graphene for interconnection at a certain spectral range by utilizing our theory, and the prediction is verified by the simulation of 90° turning of GSPPs. With the development of graphene applications in nanophotonic circuits, flexible plasmonic devices, biocompatible devices, and many other fields that may use curved GSPPs, the understanding of the property of curved GSPPs plays a key role. Thus, our results provide a promising way to clarify the bending effect of GSPPs and can precisely instruct the design work involving curved GSPPs.

ACKNOWLEDGMENT

This work is supported by the 973 Program of China (nos. 2013CB632704 and 2011CB922002) and the National Natural Science Foundation of China (no. 11204365).

REFERENCES

1. W. L. Barnes, A. Dereux, and T. W. Ebbesen, "Surface plasmon subwavelength optics," Nature **424**, 824–830 (2003).
2. Y. G. Chen, Y. H. Chen, and Z. Y. Li, "Direct method to control surface plasmon polaritons on metal surfaces," Opt. Lett. **39**, 339–342 (2014).
3. Y.-H. Chen, L. Huang, L. Gan, and Z.-Y. Li, "Wavefront shaping of infrared light through a subwavelength hole," Light Sci. Appl. **1**, e26 (2012).
4. Y.-H. Chen, M. Zhang, L. Gan, X. Wu, L. Sun, J. Liu, J. Wang, and Z.-Y. Li, "Holographic plasmonic lenses for surface plasmons with complex wavefront profile," Opt. Express **21**, 17558–17566 (2013).
5. S. Y. Liu, L. Huang, J. F. Li, C. Wang, Q. Li, H. X. Xu, H. L. Guo, Z. M. Meng, Z. Shi, and Z. Y. Li, "Simultaneous excitation and emission enhancement of fluorescence assisted by double plasmon modes of gold nanorods," J. Phys. Chem. C **117**, 10636–10642 (2013).
6. Z. Y. Li, "Optics and photonics at nanoscale: principles and perspectives," Europhys. Lett. **110**, 14001 (2015).
7. F. H. L. Koppens, D. E. Chang, and F. J. G. de Abajo, "Graphene plasmonics: a platform for strong light-matter interactions," Nano Lett. **11**, 3370–3377 (2011).
8. A. K. Geim and K. S. Novoselov, "The rise of graphene," Nat. Mater. **6**, 183–191 (2007).
9. A. N. Grigorenko, M. Polini, and K. S. Novoselov, "Graphene plasmonics," Nat. Photonics **6**, 749–758 (2012).
10. H. G. Yan, X. S. Li, B. Chandra, G. Tulevski, Y. Q. Wu, M. Freitag, W. J. Zhu, P. Avouris, and F. N. Xia, "Tunable infrared plasmonic devices using graphene/insulator stacks," Nat. Nanotechnol. **7**, 330–334 (2012).
11. L. Ju, B. S. Geng, J. Horng, C. Girit, M. Martin, Z. Hao, H. A. Bechtel, X. G. Liang, A. Zettl, Y. R. Shen, and F. Wang, "Graphene plasmonics for tunable terahertz metamaterials," Nat. Nanotechnol. **6**, 630–634 (2011).
12. W. B. Lu, W. Zhu, H. J. Xu, Z. H. Ni, Z. G. Dong, and T. J. Cui, "Flexible transformation plasmonics using graphene," Opt. Express **21**, 10475–10482 (2013).
13. A. Vakil and N. Engheta, "Transformation optics using graphene," Science **332**, 1291–1294 (2011).
14. D. R. Andersen, "Graphene-based long-wave infrared TM surface plasmon modulator," J. Opt. Soc. Am. B **27**, 818–823 (2010).
15. L. Wu, H. S. Chu, W. S. Koh, and E. P. Li, "Highly sensitive graphene biosensors based on surface plasmon resonance," Opt. Express **18**, 14395–14400 (2010).
16. Y. Yao, M. A. Kats, P. Genevet, N. F. Yu, Y. Song, J. Kong, and F. Capasso, "Broad electrical tuning of graphene-loaded plasmonic antennas," Nano Lett. **13**, 1257–1264 (2013).
17. K. S. Novoselov, V. I. Fal'ko, L. Colombo, P. R. Gellert, M. G. Schwab, and K. Kim, "A roadmap for graphene," Nature **490**, 192–200 (2012).
18. S. Aksu, M. Huang, A. Artar, A. A. Yanik, S. Selvarasah, M. R. Dokmeci, and H. Altug, "Flexible plasmonics on unconventional and nonplanar substrates," Adv. Mater. **23**, 4422–4430 (2011).
19. X. L. Zhu, W. Yan, N. A. Mortensen, and S. S. Xiao, "Bends and splitters in graphene nanoribbon waveguides," Opt. Express **21**, 3486–3491 (2013).
20. E. Forati and G. W. Hanson, "Surface plasmon polaritons on soft-boundary graphene nanoribbons and their application in switching/demultiplexing," Appl. Phys. Lett. **103**, 133104 (2013).
21. V. P. Gusynin, S. G. Sharapov, and J. P. Carbotte, "Magneto-optical conductivity in graphene," J. Phys. Condens. Matter **19**, 026222 (2007).
22. C. F. Chen, C. H. Park, B. W. Boudouris, J. Horng, B. S. Geng, C. Girit, A. Zettl, M. F. Crommie, R. A. Segalman, S. G. Louie, and F. Wang, "Controlling inelastic light scattering quantum pathways in graphene," Nature **471**, 617–620 (2011).
23. X. Y. He and R. Li, "Comparison of graphene-based transverse magnetic and electric surface plasmon modes," IEEE J. Sel. Top. Quantum Electron. **20**, C1 (2014).